



SU(3) Spin–Orbit Coupled Rotating Bose–Einstein Condensate Subject to a Gradient Magnetic Field

Guang-Ping Chen^{1,2*}, Pu Tu^{1,2}, Chang-Bing Qiao³, Jin-Xia Zhu^{1,2}, Qi Jia^{1,2} and Xiao-Fei Zhang^{4*}

¹College of Intelligent Manufacturing, Sichuan University of Arts and Science, DaZhou, China, ²Industry Technology Research Institute of Intelligent Manufacturing, Sichuan University of Arts and Science, DaZhou, China, ³College of Chemistry and Chemical Engineering, Sichuan University of Arts and Science, DaZhou, China, ⁴Department of Physics, Shaanxi University of Science and Technology, Xi'an, China

OPEN ACCESS

Edited by:

Zhaoxin Liang,
Zhejiang Normal University, China

Reviewed by:

Qing Sun,
Capital Normal University, China
Wei Yi,
University of Science and Technology
of China, China
Xiang-Fa Zhou,
University of Science and Technology
of China, China

*Correspondence:

Guang-Ping Chen
chengp205@126.com
Xiao-Fei Zhang
xtzhang_physics@163.com

Specialty section:

This article was submitted to
Optics and Photonics,
a section of the journal
Frontiers in Physics

Received: 01 September 2021

Accepted: 29 September 2021

Published: 02 November 2021

Citation:

Chen G-P, Tu P, Qiao C-B, Zhu J-X,
Jia Q and Zhang X-F (2021) SU(3)
Spin–Orbit Coupled Rotating
Bose–Einstein Condensate Subject to
a Gradient Magnetic Field.
Front. Phys. 9:768799.
doi: 10.3389/fphy.2021.768799

We consider a harmonically trapped rotating spin-1 Bose–Einstein condensate with SU(3) spin–orbit coupling subject to a gradient magnetic field. The effects of SU(3) spin–orbit coupling, rotation, and gradient magnetic field on the ground-state structure of the system are investigated in detail. Our results show that the interplay among SU(3) spin–orbit coupling, rotation, and gradient magnetic field can result in a variety of ground states, such as a vortex ring and clover-type structure. The numerical results agree well with our variational analysis results.

Keywords: Bose–Einstein condensate, SU(3) spin–orbit coupling, gradient magnetic field, rotation, GP equation

1 INTRODUCTION

Spin–orbit coupling (SOC) plays an important role in a variety of physics branches. The realization of SOC in neutral atomic gases has attracted major attention both theoretically and experimentally [1–10]. Previous works have shown that the SOC can induce a variety of topological defects, such as skyrmions and half-quantum vortices and solitons, which are useful for the design and exploration of new functional materials [11–18]. Besides the ground-state structure, the dynamic properties of the system are significantly altered in the presence of SOC due to the close relationship between the spin and motional degrees of freedom in the topological excitations [19–24].

With the development of low-temperature technology, various types of SOC, such as Rashba, Dresselhaus, Weyl, and spin–orbit angular momentum, can be realized in experiments [1, 4, 25, 26]. However, most of previous studies of SOC have focused on the type of SU(2), where the internal states are coupled to their momenta via the SU(2) Pauli matrices. Only few works consider the SU(3) SOC, where the spin operators are spanned by the Gell-Mann matrices, which is more effective in describing the internal couplings among three-component condensates, such as a spin-1 Bose–Einstein condensate (BEC). Recently, Han and his co-authors have considered a homogenous SU(3) SO-coupled Bose gas and obtained the double-quantum spin vortices [27]. On the base of their pioneering research work, Li and Chen have studied the SU(3) SO-coupled BEC confined in a harmonic plus quartic trap [28]. Very recently, the ground states of a harmonically trapped spin-1 BEC with SU(3) BEC affected by the external rotation are investigated in [29], where a clover-type ground-state structure is discovered.

Nowadays, the gradient magnetic field has attracted more and more attention. More specifically, it is found that a variety of topological defects, such as a magnetic monopole and quantum knot, and even the artificial SOC can be realized by controlling the gradient magnetic field [30–34]. Li and his co-authors have investigated the ground state of three-component BEC in the gradient magnetic field

and obtained the central Mermin–Ho vortex, magnetic monopole, and symmetry vortex lattices [35, 36]. They have also investigated the ground state of SU(2) SO-coupled BEC in the magnetic field and found that the skyrmion chain can be induced by the isotropic SU(2) SOC [37]. As far as we know, there is little study on an SU(3) SO-coupled BEC subject to both rotation and gradient magnetic field, which is what we attempt to do. In this work, we consider an SU(3) SO-coupled rotating BEC subject to a gradient magnetic field and show that the system has a rich variety of ground states. Here, we want to note that, in real experiments, it is difficult to realize a rotating BEC with fixed SOC [38–40]. To do so, we can rotate the lasers creating SOC for an isotropic trap or rotate both the lasers creating SOC and an anisotropic trap, which leads to an effective time-independent Hamiltonian, $H_{\text{eff}} = H - \Omega L_z$, describing the system in a rotating frame of Ref. [41].

The rest of this paper is organized as follows. In **Section 2**, we formulate the theoretical model describing an SU(3) SO-coupled BEC subject to both rotation and gradient magnetic field and briefly introduce the numerical method. The numerical results and its corresponding theoretical analysis through the variational approach are presented in **Section 3**. Finally, in **Section 4**, the main results of the work are summarized.

2 MODEL AND METHOD

To begin with, we consider a quasi-two-dimensional (Q2D) spin-1 BEC with SU(3) SOC [27], which is confined in a controllable magnetic field [36]. Under the mean-field approximation, the Hamiltonian of such a system can be written as [42–44]

$$H = \int d^2\mathbf{r} \left(\Psi^\dagger \left[-\frac{\hbar^2 \nabla^2}{2M} + V(\mathbf{r}) - \Omega L_z + \nu_{\text{so}} + \mathbf{g}_F \mu_B \mathbf{B}(\mathbf{r}) \cdot \mathbf{F} \right] \Psi + \frac{c_0}{2} n^2 + \frac{c_2}{2} [(n_1 - n_{-1})^2 + 2|\psi_1^* \psi_0 + \psi_0^* \psi_{-1}|^2] \right), \quad (1)$$

where $\Psi = [\psi_1(\mathbf{r}), \psi_0(\mathbf{r}), \psi_{-1}(\mathbf{r})]^T$ with $\mathbf{r} = (x, y)$ denotes the spinor order parameters of the spin-1 BEC with normalization $\int \Psi^\dagger \Psi d^2r = N$. M is the atomic mass, $n = \sum_m n_m$ with $n_m = |\psi_m(\mathbf{r})|^2$, and $m = 0, \pm 1$ is defined as the condensate density. The Q2D geometry can be realized by imposing a strong harmonic potential $V(z) = M\omega_z^2 z^2/2$ along the axial direction with $\omega_z \gg \omega_\perp$. In this case, the external trapping potential can be written as $V(r) = \frac{1}{2} M [\omega_\perp^2 (x^2 + y^2)]$, with ω_\perp being the radial trapping frequencies. For the interaction terms, the coupling parameters are given by $c_0 = \frac{4\pi\hbar^2(a_0+2a_2)}{3M}$ and $c_2 = \frac{4\pi\hbar^2(a_2-a_0)}{3M}$, where $a_{0,2}$ are two-body s -wave scattering lengths for total spins 0 and 2, respectively. $L_z = -i\hbar(x\partial_y - y\partial_x)$ is the z -component of the angular momentum, and Ω is the angular frequency of the external rotation. The vector of spin-1 matrices is defined by $\mathbf{F} = (F_x, F_y, F_z)^T$, wherein F_x, F_y , and F_z are the 3×3 Pauli spin-1 matrices.

The SU(3) SOC considered in the present work can be written as $\nu_{\text{so}} = \kappa \lambda \cdot p$, where κ is the strength of SU(3) SOC and $p = (p_x, p_y)$ represents the momentum in the Q2D space.

$\lambda = (\lambda_x, \lambda_y)$ is expressed in terms of $\lambda_x = \lambda^{(1)} + \lambda^{(4)} + \lambda^{(6)}$ and $\lambda_y = \lambda^{(2)} - \lambda^{(5)} + \lambda^{(7)}$, with $\lambda^{(i)} (i = 1, 2, \dots, 8)$ being the Gell-Mann matrices. In this case, the generators of the SU(3) group can be written as [45]

$$\lambda_x = \begin{pmatrix} 0 & 1 & 1 \\ 1 & 0 & 1 \\ 1 & 1 & 0 \end{pmatrix}, \lambda_y = \begin{pmatrix} 0 & -i & i \\ i & 0 & -i \\ -i & i & 0 \end{pmatrix}.$$

Note that the SU(3) SOC in the Hamiltonian involves all the pairwise couplings between three states. This is distinct from the SU(2) case, where the state of $\psi_1(r)$ and $\psi_{-1}(r)$ cannot be coupled directly. In real experiments, the Hamiltonian with SU(3) SOC can be realized using a similar method of Raman dressing as in the SU(2) case, where three laser beams with different polarizations and frequencies, intersecting at an angle of $2\pi/3$, are used for the Raman coupling [27]. The external magnetic field is given by $\mathbf{B}(\mathbf{r}) = B_1(x\hat{e}_x - y\hat{e}_y) + B_2z\hat{e}_z$, where the condition $B_1 = B$ is the magnetic field gradient in the 2D plane, and we focus on the case of axial bias field $B_2 = 0$. The Lande factor $g_F = -\frac{1}{2}$, and μ_B is the Bohr magneton. The ground state and dynamics of the system can be described by the following dimensionless coupled Gross–Pitaevskii equations:

$$\begin{aligned} i \frac{\partial \phi_1}{\partial t} &= \left[-\frac{1}{2} \nabla^2 + V(r) + i\Omega(x\partial_y - y\partial_x) \right. \\ &+ c_0(|\phi_1|^2 + |\phi_0|^2 + |\phi_{-1}|^2) + c_2(|\phi_1|^2 + |\phi_0|^2 - |\phi_{-1}|^2) \Big] \phi_1 \\ &+ B(x + iy)\phi_0 + c_2\phi_{-1}^*\phi_0^2 - \kappa(i\partial_x + \partial_y)\phi_0 + \kappa(\partial_y - i\partial_x)\phi_{-1}, \\ i \frac{\partial \phi_0}{\partial t} &= \left[-\frac{1}{2} \nabla^2 + V(r) + i\Omega(x\partial_y - y\partial_x) + c_0(|\phi_1|^2 + |\phi_0|^2 + |\phi_{-1}|^2) \right. \\ &+ c_2(|\phi_1|^2 + |\phi_{-1}|^2) \Big] \phi_0 + B(x - iy)\phi_1 + B(x + iy)\phi_{-1} \\ &+ 2c_2\phi_0^*\phi_1\phi_{-1} + \kappa(\partial_y - i\partial_x)\phi_1 - \kappa(\partial_y + i\partial_x)\phi_{-1}, \\ i \frac{\partial \phi_{-1}}{\partial t} &= \left[-\frac{1}{2} \nabla^2 + V(r) + i\Omega(x\partial_y - y\partial_x) + c_0(|\phi_1|^2 + |\phi_0|^2 + |\phi_{-1}|^2) \right. \\ &+ c_2(|\phi_{-1}|^2 + |\phi_0|^2 - |\phi_1|^2) \Big] \phi_{-1} + B(x - iy)\phi_0 + c_2\phi_1^*\phi_0^2 \\ &\left. - \kappa(i\partial_x + \partial_y)\phi_1 + \kappa(\partial_y - i\partial_x)\phi_0, \right. \quad (2) \end{aligned}$$

where the length and time units are chosen as $l_\perp = [\hbar/M\omega_\perp]^{1/2}$ and ω_\perp^{-1} and the normalized wave functions $\phi_j = l_\perp \psi_j / \sqrt{N}$, satisfying the condition $\int \sum_{j=-1}^1 |\phi_j|^2 dx dy = 1$. The contact interaction parameters are scaled by $\Omega = \Omega/\omega_\perp$, $\kappa = \kappa/(\hbar\omega_\perp l_\perp)$, $B = Bg_F\mu_B l_\perp/(\hbar\omega_\perp)$, and $c_{0,2} = c_{0,2}N/(\hbar\omega_\perp l_\perp^2)$. The ground state of the system can be obtained by using the standard imaginary-time propagation combined with the finite difference methods [46–48]. In our numerical simulations, we prepare with different initial states and then propagate the wave functions in imaginary time to make sure that we proceed to a sufficiently large number of time steps, which guarantees that we have reached a steady state.

3 RESULTS AND DISCUSSIONS

In what follows, we will perform a detailed numerical study of the effects of system parameters on the ground-state structure. The

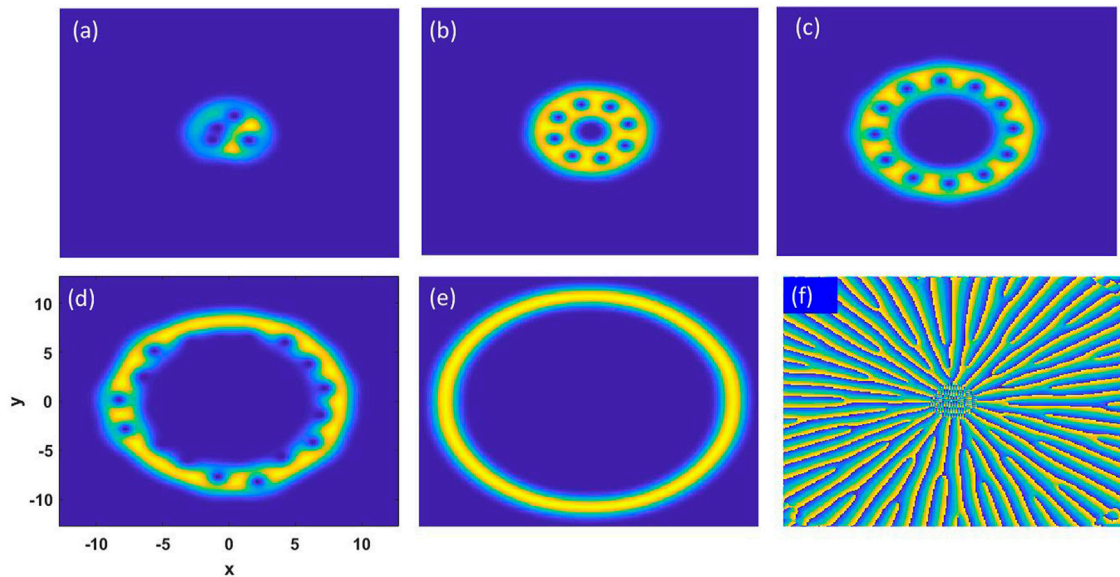


FIGURE 1 | Typical ground-state structures of a rotating BEC as a function of the gradient magnetic field in the absence of SU(3) spin–orbit coupling. **(A)–(E)** Density distributions of component 1 for different gradient magnetic fields: **(A)** $B = 0$, **(B)** $B = 1$, **(C)** $B = 2$, **(D)** $B = 3$, and **(E)** $B = 4$. **(F)** The corresponding phase distribution of **(C)**. Other parameters are fixed as $c_0 = 100$, $c_2 = 3$, $\Omega = 0.7$, and $\kappa = 0$, and the scale of each figure is $[-12.8, 12.8]$ in units of $I_{\perp} = [\hbar/M\omega_{\perp}]^{1/2}$.

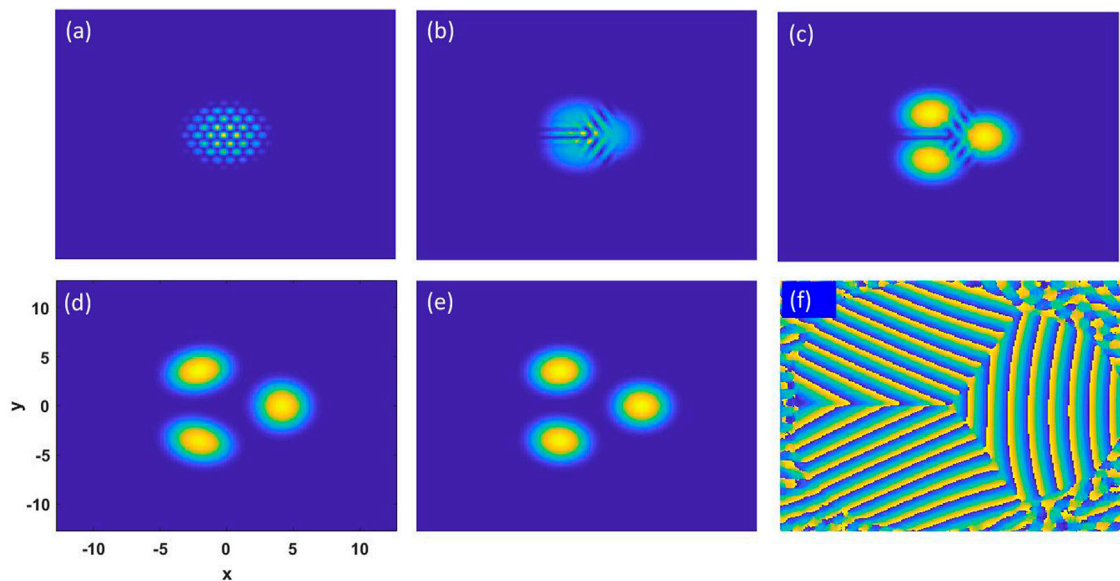
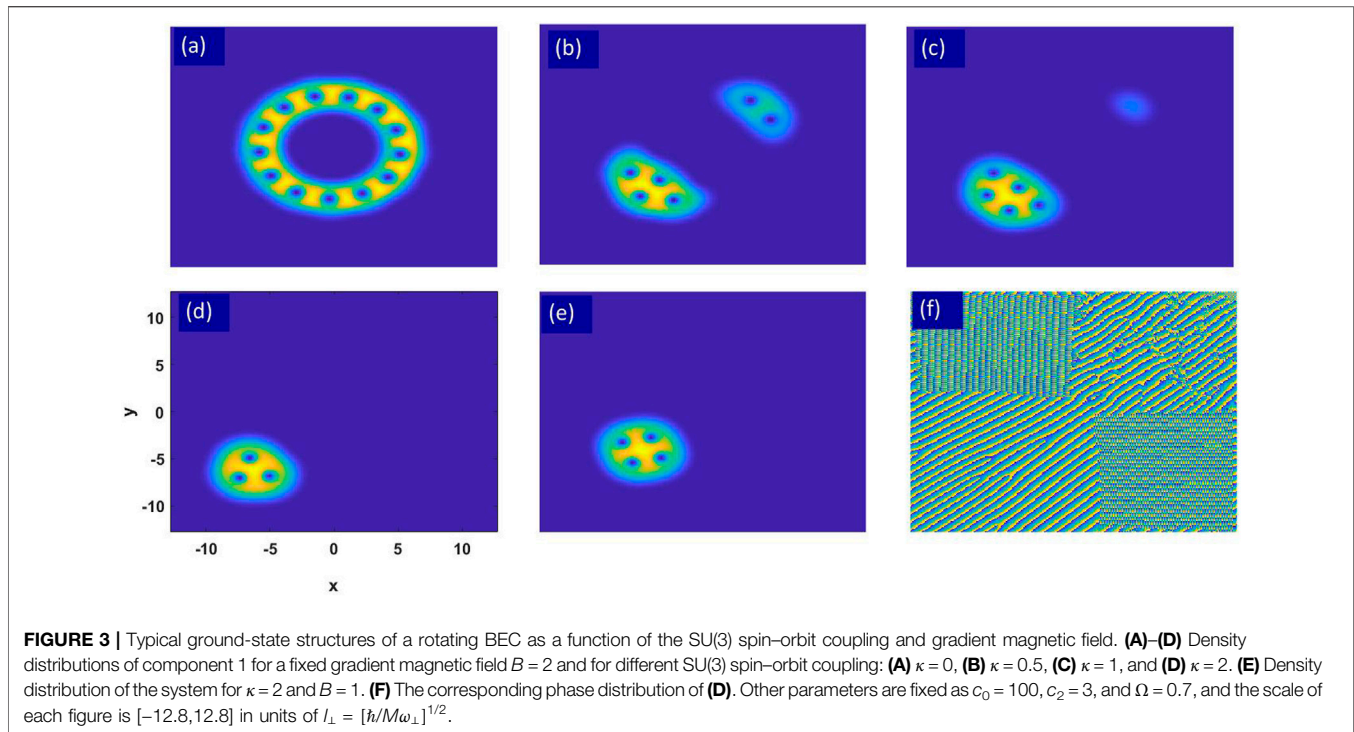


FIGURE 2 | Typical ground-state structures of an SU(3) spin–orbit-coupled BEC as a function of SU(3) spin–orbit coupling and gradient magnetic field in the absence of rotation. **(A)–(D)** Density distributions of component 1 for fixed SU(3) spin–orbit coupling $\kappa = 3$ and for different gradient magnetic fields: **(A)** $B = 0$, **(B)** $B = 1$, **(C)** $B = 2$, and **(D)** $B = 3$. **(E)** Density distribution of the system for $B = 3$ and $\kappa = 5$. **(F)** The corresponding phase distribution of **(D)**. Other parameters are fixed as $c_0 = 100$, $c_2 = 3$, and $\Omega = 0$, and the scale of each figure is $[-12.8, 12.8]$ in units of $I_{\perp} = [\hbar/M\omega_{\perp}]^{1/2}$.

richness of the present system lies in the large number of free parameters, which include the spin-dependent and spin-independent contact interactions, SU(3) SOC, rotation, and gradient field. To highlight the effects of the SOC, rotation, and gradient field, we focus on the antiferromagnetic

condensate with $c_2 > 0$ and fix the contact coupling parameters $c_0 = 100$ and $c_2 = 3$.

We first consider the system without SOC and fix the rotation frequency as $\Omega = 0.7$. The typical density and phase distributions of such a system are shown in **Figure 1** for different gradient



magnetic fields, where only component 1 is shown as the other two components show similar behavior. In the absence of both gradient field ($B = 0$) and SU(3) SOC ($\kappa = 0$), the system is located at the center of the external harmonic potential, and no other lumps are formed. In this case, discrete vortices are formed due to the external rotation, but no vortex lattice can be formed due to the small contact interactions, as shown in **Figure 1A**. In the presence of a gradient magnetic field, the density distribution of the system shows a ring structure, and the size of center hole increases with the strength of the gradient magnetic field, as shown in **Figures 1B,C** for $B = 1$ and $B = 2$, respectively. In these cases, a vortex ring is formed along the ring direction (see **Figure 1F** for the phase distribution of **Figure 1C**), and the number of vortex also increases with the gradient magnetic field. Furthermore, if we increase the strength of gradient magnetic to $B = 3$ (see **Figure 1D**), most of vortices begin to move into the central hole, and the vortex ring is gradually destroyed. Upon increasing the gradient field to $B = 4$, all the vortices move to the central hole and form a giant vortex at the center of the trapping potential. In this case, no visible vortex remains, as shown in **Figure 1E**. Comparing **Figures 1A–E**, it is found that the radius of the ring increases with the gradient magnetic field.

Now, we turn our attention to the combined effects of SU(3) SOC and gradient magnetic on the ground-state structure of the system and thus set $\Omega = 0$. **Figure 2** shows the typical density and phase distributions of the system for the varying SU(3) SOC and gradient magnetic field. Previous studies on the SU(3) SOC Bose gases have shown that the triangular lattice structure is energy favorable for both

homogeneous and confined systems [27, 29]. In the present system, we find a similar triangular lattice structure in the absence of the gradient magnetic field ($B = 0$), as shown in **Figure 2A**. In the presence of a gradient magnetic field, it is found that, with the increasing strength of the gradient magnetic field, the triangular lattice structure is gradually destroyed. In addition, the system evolves into three parts in space and eventually into a clover-type structure, as shown in **Figures 2B–D** for $B = 1, 2, 3$, respectively. Here, we want to note that a similar clover-type structure has been previously discovered in an SU(3) SO-coupled Bose gas with rotation [29]. However, the clover-type structure found in the present work is induced by the combined effects of both SU(3) SOC and a gradient magnetic field, which give us another way to realize the clover-type structure in a non-rotating system. It is interesting to observe that the distance among such three space parts of the clover-type structure is unchanged if we increase the strength of SU(3) SOC but fix the strength of the gradient magnetic field, as shown in **Figures 2D,E** for $B = 3, \kappa = 3$ and $B = 3, \kappa = 5$, respectively. If we look at the phase distribution of the clover-type structure, as shown in **Figure 2F** for **Figure 2D**, it is easy to find that the local lump is in the plane wave phase, which is consistent with our previous results on the SU(3) SO-coupled system [27].

Finally, we move to the combined effects of SU(3) SOC, rotation, and the gradient magnetic field on the ground-state structure of the system. To highlight the effect of SU(3) SOC, we further fix $\Omega = 0.7$. **Figure 3** shows the typical ground-state structures of a rotating BEC as a function of the SU(3) SOC and gradient magnetic field. In the absence of SU(3) SOC, the system

shows a ring structure with a vortex ring (see **Figure 3A** for $B = 2$ and $\kappa = 0$), which is consistent with that reported in **Figure 1C**. In the presence of SU(3) SOC, it is found that the annular structure is destroyed even for a small SU(3) SOC, as shown in **Figure 3B** for $\kappa = 0.5$ and $B = 2$, where two asymmetry lumps with visible vortices are formed. Further increasing the strength of SU(3) SOC, this tendency is becoming more and more obvious, and eventually, the system evolves into a single lump, as shown in **Figures 3C,D, and F** (the corresponding phase distribution of (**Figure 3D**)) for $\kappa = 1$ and $\kappa = 2$, respectively. This is different from the phase diagram in [38], where the density distributions show some symmetry and the center of mass of the system is still around the center of the trap (which also can be seen from their momentum distributions). For the present case, the symmetry of the system is further broken and the center of mass of the system deviates from the center of the trap. Actually, such difference can be understood by the fact that the SU(3) SO-coupled system has three discrete minima in the single-particle energy spectrum, and the number and weight of such three minima are selected for different strengths of SOC. Similar to the former case, it is interesting to observe that the distance between the lump and the center of trapping potential increases with the gradient magnetic field (see **Figure 3E** for $B = 1$ and $\kappa = 2$). Here, we want to note that we have also calculated other rotation frequencies, and the results show similar behavior.

To give a clearer understanding of the above results, we employ the variational method and analytically calculate the possible ground state. We begin with the single-particle energy spectrum of the system, which can be obtained by diagonalizing the kinetic energy and SOC terms. It is found that there exist three discrete minima residing on the vertices of an equilateral triangle in the momentum space. As discussed in [27], a threefold-degenerate plane wave ground state is selected as the ground state for a ferromagnetic condensate with SU(3) SOC, while three discrete minima with unequal (equal) weights are selected for the antiferromagnetic case. Consequently, the variational wave function can be written as $\Psi = \Psi_1 + \Psi_2 + \Psi_3$, where

$$\begin{aligned} \Psi_1 &= \frac{1}{\sqrt{3}} \begin{pmatrix} 1 \\ 1 \\ 1 \end{pmatrix} e^{-i2\kappa x}, \\ \Psi_2 &= \frac{1}{\sqrt{3}} \begin{pmatrix} e^{-i\pi/3} \\ e^{i\pi/3} \\ e^{i\pi} \end{pmatrix} e^{i\kappa(x-\sqrt{3}y)}, \\ \Psi_3 &= \frac{1}{\sqrt{3}} \begin{pmatrix} e^{i\pi/3} \\ e^{-i\pi/3} \\ e^{i\pi} \end{pmatrix} e^{i\kappa(x+\sqrt{3}y)}, \end{aligned} \tag{3}$$

where Ψ_1, Ψ_2 , and Ψ_3 are the wave functions corresponding to the three minima of the single-particle spectrum, $(-2\kappa, 0)$, $(\kappa, -\sqrt{3})$, and $(\kappa, \sqrt{3})$. Substituting these ansatzes into **Equation 1**, we can calculate the energy for each minimum in the momentum space as follows:

$$\begin{aligned} E_1 &= \frac{1}{2} \left(x - \frac{4}{3}B\right)^2 + \frac{1}{2}y^2 - \frac{8}{9}B^2, \\ E_2 &= \frac{1}{2} \left(x + \frac{2}{3}B\right)^2 + \frac{1}{2} \left(y + \frac{2\sqrt{3}}{3}B\right)^2 - \frac{8}{9}B^2, \\ E_3 &= \frac{1}{2} \left(x + \frac{2}{3}B\right)^2 + \frac{1}{2} \left(y - \frac{2\sqrt{3}}{3}B\right)^2 - \frac{8}{9}B^2. \end{aligned} \tag{4}$$

It is found that the minimum energies are equal to $-\frac{8}{9}B^2$. Consequently, there also exist three points in real space, that is, $(\frac{4}{3}B, 0)$, $(-\frac{2}{3}B, -\frac{2\sqrt{3}}{3}B)$, and $(-\frac{2}{3}B, \frac{2\sqrt{3}}{3}B)$. In this case, particles can condense at such three real space points, and the three lumps locate at the x -axis, the second quadrant and the third quadrant. In addition, we find that these positions are only related to the gradient magnetic field B and show independence with SU(3) SOC κ . All the results are consistent with those reported in **Figure 2**. When the rotation is included, we have

$$\begin{aligned} E_1 &= \frac{1}{2} \left(x - \frac{4}{3}B\right)^2 + \frac{1}{2} (y - 2\kappa\Omega y)^2 - 2\kappa^2\Omega^2 - \frac{8}{9}B^2, \\ E_2 &= \frac{1}{2} \left(x + \sqrt{3}\kappa\Omega + \frac{2}{3}B\right)^2 + \frac{1}{2} \left(y + \kappa\Omega + \frac{2\sqrt{3}}{3}B\right)^2 \\ &\quad - 2\Omega^2\kappa^2 - \frac{8}{9}B^2 - \frac{4\sqrt{3}}{3}\Omega\kappa B, \\ E_3 &= \frac{1}{2} \left(x - \sqrt{3}\kappa\Omega + \frac{2}{3}B\right)^2 + \frac{1}{2} \left(y + \kappa\Omega - \frac{2\sqrt{3}}{3}B\right)^2 - 2\Omega^2\kappa^2 \\ &\quad - \frac{8}{9}B^2 + \frac{4\sqrt{3}}{3}\Omega\kappa B. \end{aligned} \tag{5}$$

In this case, the second equation has the minimum energy $E_{2min} = -2\Omega^2\kappa^2 - \frac{8}{9}B^2 - \frac{4\sqrt{3}}{3}\Omega\kappa B$. Therefore, all particles condense at a single real space point $(-\sqrt{3}\kappa\Omega - \frac{2}{3}B, -\kappa\Omega - \frac{2\sqrt{3}}{3}B)$, and the distance between the lump and the center of trapping potential increases with the gradient magnetic field B , which are consistent with those reported in **Figure 3**.

4 CONCLUSION

We have investigated the ground-state structure of a harmonically trapped rotating spin-1 BEC with SU(3) SOC subject to a gradient magnetic field. In the absence of SU(3) SOC, the system shows an annular structure, where a vortex ring is formed. In the absence of rotation, it is found that the clover-type structure discovered in the previous work can also be induced by the combined effects of

SU(3) SOC and gradient magnetic field, and their distance shows sole dependence on the gradient magnetic field. When the rotation is included, we found that only one lump is formed in the three quadrants, and the distance between the lump and the center of trapping potential increases with the gradient magnetic field. Finally, we have employed the variational method and analytically calculated the possible ground state, which agrees well with our numerical simulations.

DATA AVAILABILITY STATEMENT

The raw data supporting the conclusions of this article will be made available by the authors, without undue reservation.

REFERENCES

- Lin Y-J, Jiménez-García K, and Spielman IB. Spin-orbit-coupled Bose-Einstein Condensates. *Nature* (2011) 471:83–6. doi:10.1038/nature09887
- Wang P, Yu ZQ, Fu Z, Miao J, Huang L, Chai S, et al. Spin-orbit Coupled Degenerate Fermi Gases. *Phys Rev Lett* (2012) 109:095301. doi:10.1103/PhysRevLett.109.095301
- Cheuk LW, Sommer AT, Hadzibabic Z, Yefsah T, Bakr WS, and Zwierlein MW. Spin-Injection Spectroscopy of a Spin-Orbit Coupled Fermi Gas. *Phys Rev Lett* (2012) 109:095302. doi:10.1103/PhysRevLett.109.095302
- Huang L, Meng Z, Wang P, Peng P, Zhang S-L, Chen L, et al. Experimental Realization of Two-Dimensional Synthetic Spin-Orbit Coupling in Ultracold Fermi Gases. *Nat Phys* (2016) 12:540–4. doi:10.1038/nphys3672
- Wu Z, Zhang L, Sun W, Xu X-T, Wang B-Z, Ji S-C, et al. Realization of Two-Dimensional Spin-Orbit Coupling for Bose-Einstein Condensates. *Science* (2016) 354:83–8. doi:10.1126/science.aaf6689
- Kolkowitz S, Bromley SL, Bothwell T, Wall ML, Marti GE, Koller AP, et al. Spin-orbit-coupled Fermions in an Optical Lattice Clock. *Nature* (2017) 542:66–70. doi:10.1038/nature20811
- Li J-R, Lee J, Huang W, Burchesky S, Shteynas B, Top FÇ, et al. A Stripe Phase with Supersolid Properties in Spin-Orbit-Coupled Bose-Einstein Condensates. *Nature* (2017) 543:91–4. doi:10.1038/nature21431
- Galitski V, and Spielman IB. Spin-orbit Coupling in Quantum Gases. *Nature* (2013) 494:49–54. doi:10.1038/nature11841
- Zhai H. Spin-orbit Coupled Quantum Gases. *Int J Mod Phys B* (2012) 26:1230001. doi:10.1142/s0217979212300010
- Zhai H. Degenerate Quantum Gases with Spin-Orbit Coupling: A Review. *Rep Prog Phys* (2015) 78:026001. doi:10.1088/0034-4885/78/2/026001
- Wu C, Mondragon-Schem I, and Zhou XF. Unconventional Bose-Einstein Condensations from Spin-Orbit Coupling. *Chin Phys Lett* (2011) 108:010402. doi:10.1088/0256-307x/28/9/097102
- Hu H, Ramachandran B, Pu H, and Liu XJ. Spin-orbit Coupled Weakly Interacting Bose-Einstein Condensates in Harmonic Traps. *Phys Rev Lett* (2012) 108:010402. doi:10.1103/PhysRevLett.108.010402
- Wang C, Gao C, Jian C-M, and Zhai H. Spin-orbit Coupled Spinor Bose-Einstein Condensates. *Phys Rev Lett* (2010) 105:160403. doi:10.1103/physrevlett.105.160403
- Ho T-L, and Zhang S. Bose-Einstein Condensates with Spin-Orbit Interaction. *Phys Rev Lett* (2011) 107:150403. doi:10.1103/physrevlett.107.150403
- Fung T, Poon J, and Liu XJ. Quantum Spin Dynamics in a Spin-Orbit-Coupled Bose-Einstein Condensate. *Phys Rev A* (2016) 93:063420. doi:10.1103/physreva.93.063420
- Hu H, Ramachandran B, Pu H, Liu XJ, Drummond PD, and Hu H. Spin-orbit Coupled Weakly Interacting Bose-Einstein Condensates in Harmonic Traps. *Phys Rev Lett* (2012) 108:010402. doi:10.1103/PhysRevLett.108.010402
- Kato M, Zhang XF, Sasaki D, and Saito H. Twisted Spin Vortices in a Spin-1 Bose-Einstein Condensate with Rashba Spin-Orbit Coupling and Dipole-Dipole Interaction. *Phys Rev A* (2016) 94:043633. doi:10.1103/physreva.94.043633
- Liu Y, Holder T, and Yan B. Chirality-Induced Giant Unidirectional Magnetoresistance in Twisted Bilayer Graphene. *The Innovation* (2021) 2:100085. doi:10.1016/j.xinn.2021.100085
- Han W, Juzeliūnas G, Zhang W, and Liu WM. Supersolid with Nontrivial Topological Spin Textures in Spin-Orbit-Coupled Bose Gases. *Phys Rev A* (2015) 91:013607. doi:10.1103/physreva.91.013607
- Zhang XF, Kato M, Han W, Zhang SG, and Saito H. Spin-orbit-coupled Bose-Einstein Condensates Held under a Toroidal Trap. *Phys Rev A* (2017) 95:033620. doi:10.1103/physreva.95.033620
- Wen L, Sun Q, Wang HQ, Ji AC, and Liu WM. Ground State of Spin-1 Bose-Einstein Condensates with Spin-Orbit Coupling in Zeeman Field. *Phys Rev A* (2012) 86:043602. doi:10.1103/physreva.86.043602
- Wen L, Sun Q, Chen Y, Wang DS, Hu J, Chen H, et al. Motion of Solitons in One-Dimensional Spin-Orbit-Coupled Bose-Einstein Condensates. *Phys Rev A* (2016) 94:061602. doi:10.1103/physreva.94.061602
- Sun Q, Wen L, Liu WM, Juzeliūnas G, and Ji AC. Tunneling-assisted Spin-Orbit Coupling in Bilayer Bose-Einstein Condensates. *Phys Rev A* (2015) 91:033619. doi:10.1103/physreva.91.033619
- Sakaguchi H, Li B, and Malomed BA. Creation of Two-Dimensional Composite Solitons in Spin-Orbit-Coupled Self-Attractive Bose-Einstein Condensates in Free Space. *Phys Rev E Stat Nonlin Soft Matter Phys* (2014) 89:032920. doi:10.1103/PhysRevE.89.032920
- Anderson BM, Juzeliūnas G, Galitski VM, and Spielman IB. Synthetic 3D Spin-Orbit Coupling. *Phys Rev Lett* (2012) 108:235301. doi:10.1103/physrevlett.108.235301
- Chen H-R, Lin K-Y, Chen P-K, Chiu N-C, Wang J-B, Chen C-A, et al. Spin-Orbital-Angular-Momentum Coupled Bose-Einstein Condensates. *Phys Rev Lett* (2018) 121:113204. doi:10.1103/physrevlett.121.113204
- Han W, Zhang XF, Song SW, Saito H, Zhang W, Liu WM, et al. Double-quantum Spin Vortices in SU(3) Spin-Orbit-Coupled Bose Gases. *Phys Rev A* (2016) 94:033629. doi:10.1103/physreva.94.033629
- Li CH, Qu C, Niffenegger RJ, Wang SJ, He M, Blasing DB, et al. Spin Current Generation and Relaxation in a Quenched Spin-Orbit-Coupled Bose-Einstein Condensate. *Nat Commun* (2019) 10:375–02. doi:10.1038/s41467-018-08119-4
- Peng P, Li G-Q, Wang B-H, and Cao Z-Z. Exotic Ground States in a SU(3) Spin-Orbit Coupled Spin-1 Bose-Einstein Condensate under Rotation. *Chaos, Solitons & Fractals* (2020) 141:110332. doi:10.1016/j.chaos.2020.110332
- Anderson BM, Spielman IB, and Juzeliūnas G. Magnetically Generated Spin-Orbit Coupling for Ultracold Atoms. *Phys Rev Lett* (2013) 111:125301. doi:10.1103/physrevlett.111.125301
- Xu ZF, You L, and Ueda M. Atomic Spin-Orbit Coupling Synthesized with Magnetic-Field-Gradient Pulses. *Phys Rev A* (2013) 87:063634. doi:10.1103/physreva.87.063634
- Aidelsburger M, Atala M, Lohse M, Barreiro JT, Barreiro B, and Bloch I. Realization of the Hofstadter Hamiltonian with Ultracold Atoms in Optical Lattices. *Phys Rev Lett* (2013) 111:185301. doi:10.1103/physrevlett.111.185301

AUTHOR CONTRIBUTIONS

All authors listed have made a substantial, direct, and intellectual contribution to the work and approved it for publication.

FUNDING

This work was supported by the National Natural Science Foundation of China under Grant Nos. 12075163, 12175129, 11775253, 12175027, and 11875010; the Dazhou Science and Technology Bureau under Grant No. 2019CYR0001; and the Natural Science Foundation of Chongqing under Grant No. cstc2019cyj-msxmX0217.

33. Kennedy CJ, Siviloglou GA, Miyake H, Burton WC, and Ketterle W. Spin-orbit Coupling and Quantum Spin Hall Effect for Neutral Atoms without Spin Flips. *Phys Rev Lett* (2013) 111:225301. doi:10.1103/physrevlett.111.225301
34. Ray MW, Ruokokoski E, Kandel S, Möttönen M, and Hall DS. Observation of Dirac Monopoles in a Synthetic Magnetic Field. *Nature* (2014) 505:657–60. doi:10.1038/nature12954
35. Li J, Yu YM, Zhuang L, and Liu WM. Dirac Monopoles with a Polar-Core Vortex Induced by Spin-Orbit Coupling in Spinor Bose-Einstein Condensates. *Phys Rev A* (2017) 95:043633. doi:10.1103/physreva.95.043633
36. Liu Jing-Si JS, Li Ji J, and Liu Wu-Ming WM. Ground State of a Rotating Bose-Einstein Condensate with In-Plane Quadrupole Field. *wlxb* (2017) 66:130305. doi:10.7498/aps.66.130305
37. Li Ji J, and Liu Wu-Ming WM. Ground State of Spin-Orbit Coupled Rotating Two-Component Bose-Einstein Condensate in Gradient Magnetic Field. *wlxb* (2018) 67:110302. doi:10.7498/aps.67.20180539
38. Radic J, Sedrakyan TA, Spielman IB, and Galitski V. Vortices in Spin-Orbit-Coupled Bose-Einstein Condensates. *Phys Rev A* (2011) 84:063604. doi:10.1103/physreva.84.063604
39. Zhou XF, Zhou J, and Wu CJ. Vortex Structures of Rotating Spin-Orbit-Coupled Bose-Einstein Condensates. *Phys Rev A* (2011) 84:063624. doi:10.1103/physreva.84.063624
40. Xu X-Q, and Han JH. Spin-Orbit Coupled Bose-Einstein Condensate under Rotation. *Phys Rev Lett* (2011) 107:200401. doi:10.1103/physrevlett.107.200401
41. Liu CF, Juzeliūnas G, and Liu WM. Spin-orbit Coupling Manipulating Composite Topological Spin Textures in Atomic-Molecular Bose-Einstein Condensates. *Phys Rev A* (2017) 95:023624. doi:10.1103/physreva.95.023624
42. Liu CF, and Liu WM. Spin-orbit-coupling-induced Half-Skyrmion Excitations in Rotating and Rapidly Quenched Spin-1 Bose-Einstein Condensates. *Phys Rev A* (2012) 86:033602. doi:10.1103/physreva.86.033602
43. Justin L, Magnus OB, and Ruostekoski J. Energetically Stable Singular Vortex Cores in an Atomic Spin-1 Bose-Einstein Condensate. *Phys Rev A* (2012) 86:013613. doi:10.1103/physreva.86.013613
44. Ji AC, Liu WM, Song JL, and Zhou F. Dynamical Creation of Fractionalized Vortices and Vortex Lattices. *Phys Rev Lett* (2008) 101:010402. doi:10.1103/PhysRevLett.101.010402
45. Arfken GB, Webber HJ, and Hrris FE. *Mathematical Methods for Physicists*. 7th ed.. New York: Academic Press (2000).
46. Bao WZ, and Du Q. Computing the Ground State Solution of Bose-Einstein Condensates by Normalized Gradient Flow. *SIAM J SCI Comput* (2014) 25:1674. doi:10.1137/s1064827503422956
47. Zhang XF, Dong RF, Liu T, Liu WM, and Zhang SG. Spin-orbit-coupled Bose-Einstein Condensates Confined in Concentrically Coupled Annular Traps. *Phys Rev A* (2012) 86:063628. doi:10.1103/physreva.86.063628
48. Chen S-L, Wang L-X, Wen L, Dai C-Q, Liu J-K, and Zhang X-F. Stripe-on-plane-wave Phase of a Binary Dipolar Bose Gases with Soft-Core Long-Range Interactions. *Optik* (2021) 247:167932. doi:10.1016/j.ijleo.2021.167932

Conflict of Interest: The authors declare that the research was conducted in the absence of any commercial or financial relationships that could be construed as a potential conflict of interest.

Publisher's Note: All claims expressed in this article are solely those of the authors and do not necessarily represent those of their affiliated organizations, or those of the publisher, the editors, and the reviewers. Any product that may be evaluated in this article, or claim that may be made by its manufacturer, is not guaranteed or endorsed by the publisher.

Copyright © 2021 Chen, Tu, Qiao, Zhu, Jia and Zhang. This is an open-access article distributed under the terms of the Creative Commons Attribution License (CC BY). The use, distribution or reproduction in other forums is permitted, provided the original author(s) and the copyright owner(s) are credited and that the original publication in this journal is cited, in accordance with accepted academic practice. No use, distribution or reproduction is permitted which does not comply with these terms.